Available online at www.sciencedirect.com
ScienceDirect
Polymer 48 (2007) 7279–7290
polymer
www.elsevier.com/locate/polymer

Solvent induced morphologies of poly(methyl methacrylate-*b*-ethylene oxide-*b*-methyl methacrylate) triblock copolymers synthesized by atom transfer radical polymerization

Daniel J. Siegwart [a], Wei Wu [a], Monisha Mandalaywala [a], Magi Tamir [b], Traian Sarbu [a], Michael S. Silverstein [b], Tomasz Kowalewski [a], Jeffrey O. Hollinger [c], Krzysztof Matyjaszewski [a,*]

[a] *Center for Macromolecular Engineering, Department of Chemistry, Carnegie Mellon University, 4400 Fifth Avenue, Pittsburgh, PA 15213, United States*
[b] *Department of Materials Engineering, Technion – Israel Institute of Technology, Haifa 32000, Israel*
[c] *Bone Tissue Engineering Center, 125 Smith Hall, Carnegie Mellon University, 5000 Forbes Avenue, Pittsburgh, PA 15213, United States*

Received 19 May 2007; received in revised form 30 September 2007; accepted 1 October 2007
Available online 12 October 2007

Abstract

Poly(methyl methacrylate-*b*-ethylene oxide-*b*-methyl methacrylate) (PMMA–PEO–PMMA) triblock copolymers were synthesized using atom transfer radical polymerization (ATRP) and halogen exchange ATRP. PEO-based macroinitiators with molecular weight from $M_n = 2000$ to 35,800 g/mol were used to initiate the polymerization of MMA to obtain copolymers with molecular weight up to $M_n =$ 82,000 g/mol and polydispersity index (PDI) less than 1.2. The macroinitiators and copolymers were characterized by gel permeation chromatography (GPC) and nuclear magnetic resonance (NMR) spectroscopy. The melting temperature and glass transition temperature of the copolymers were measured by differential scanning calorimetry (DSC). Crystallinities of the PEO blocks were determined from the WAXS patterns of both homopolymers and block copolymers, which revealed the fragmentation of PEO blocks due to the folding of the PMMA chains. Interestingly, the fragmentation was less pronounced when cast on surfaces compared to that in bulk, as measured by GISAXS. Solvent casting was used to control the morphology of the copolymers, permitting the formation of various states including amorphous, induced micellar with a PMMA core and flower-like PEO arms, and a cross-linked gel. Atomic force microscopy (AFM) was used to visualize the different copolymer morphologies, showing micellar and amorphous states.

Keywords: Atom transfer radical polymerization (ATRP); Block copolymers; Atomic force microscopy (AFM)

1. Introduction

Atom transfer radical polymerization (ATRP) is one of the most versatile techniques among the several controlled/living radical polymerization (CRP) processes [1–8]. CRP techniques offer unprecedented control over macromolecular structure and allow for the synthesis of uniform polymers with unique structures from a large assortment of monomers. Because many physical properties are influenced by molecular architectures that CRP can control (including copolymer topology [9–14], microstructure [15–18], and functionality [19]), these methods can be used to produce materials with targeted properties.

ATRP allows for facile, reproducible, and highly controlled synthesis of triblock copolymers capable of forming ordered morphologies [20–23]. The unique feature of poly(methyl methacrylate) (PMMA) and poly(ethylene oxide) (PEO) triblock copolymer system described here is the miscibility of the constituent blocks, which contrasts it from more common immiscible phase separating systems.

The crystallizability of PEO makes the triblock PMMA–PEO–PMMA system more interesting. Melt miscible systems containing crystallizable components are known to exhibit

* Corresponding author. Tel.: +1 412 268 3209; fax: +1 412 268 6897.
E-mail address: km3b@andrew.cmu.edu (K. Matyjaszewski).

0032-3861/$ - see front matter © 2007 Elsevier Ltd. All rights reserved.
doi:10.1016/j.polymer.2007.10.009

complex dependence of their structure on thermal/processing history [24]. The possibility to control the ultimate structure of the material by utilizing such effects was one of the motivations of the work described here. With regard to simple blends, the segmental and local dynamics of amorphous blends of PMMA and PEO have been investigated using dielectric relaxation spectroscopy [25]. The binary blend of PEO and atactic PMMA was examined using hot-stage AFM in conjunction with differential scanning calorimetry and optical microscopy [24]. It was possible to follow the non-uniform melting process and attribute this effect to the presence of lamellae having different thicknesses. The crystallization process of PEO from the miscible melt was also followed in real time. Additionally, PEO–PMMA blends were cast from chloroform and benzene, but not from a polar solvent [26]. PMMA and PEO form a single-phase blend in the melt [27]. The miscibility is strongly influenced by the tacticity of PMMA. Atactic and syndiotactic PMMA have been found to be incorporated into the amorphous phase between the crystalline PEO lamellae, whereas in blends with isotactic PMMA, the structure consisted of alternated crystalline and amorphous lamellae of PEO, with the PMMA segregated in interfibrillar regions [28].

Despite the apparent miscibility, well defined morphologies have been observed in the block copolymers of PMMA and PEO. The isothermal crystallization of the PEO block in a linear diblock copolymer of PMMA–PEO has been previously reported using optical microscopy and differential scanning calorimetry (DSC) [29]. DSC was also employed to investigate the crystallinity and miscibility in PEO/cross-linked PMMA semi-interpenetrating networks (IPNs) [30,31]. The crystallinity of PEO in the semi-IPN was found to depend upon the cross-linking density of PMMA as well as on the overall content of PEO. The crystallinity of PEO has also been investigated for triblock copolymers [32,33] and other comparable systems such as that of PLA–PEO–PLA copolymers [34]. Applications of these degradable, physically cross-linked hydrogels include drug delivery, tissue adhesives, and orthopedic implants [35–37].

Solvent induced ordering of diblock copolymer mixtures with homopolymers was reported and visualized by AFM [38]. The AFM studies further demonstrated that solvent casting is a simple and powerful method to control the material morphology.

PMMA–PEO–PMMA triblock copolymers have been prepared in a relatively uncontrolled manner by reductive amination coupling of preformed aldehyde-terminated PEO and amine-terminated PMMA [39]. These materials were intended for use as highly permeable biocompatible encapsulating materials for mammalian cells, however, the obtained polymers had high polydispersity. In contrast, copolymers prepared in the present work were well defined, owing to the control of polymerization afforded by ATRP. Block copolymers were synthesized using macroinitiator PEO chains in which terminal hydroxyl groups were converted to bromoester serving as ATRP initiator. Similar PEO macroinitiators were used in the past to prepare other block copolymers or star copolymers by chain extension with MMA [40–45], butyl methacrylate [46], hydroxyethyl methacrylate [47], and styrene [48]. Halogen exchange ATRP [16,20,49] was employed to improve control, and the conditions were optimized to yield well defined block copolymers. The resulting materials were studied as bulk powders and as thin films prepared using different solvent casting conditions. Solvent casting has been also used to induce micelles [50–52] with a PMMA core and flower-like PEO chains on the exterior of the micelle. Interest in micellized systems was primarily driven by their potential usefulness for drug delivery through encapsulation of hydrophobic drugs in the interior of the micelles. Linking between PEO exterior loops made it also possible to prepare water-swellable gels, which might be useful for tissue engineering.

Various techniques were employed to characterize the resulting triblock copolymers. The crystallinity of PEO blocks in homopolymers and copolymers was determined by wide-angle X-ray scattering (WAXS) and DSC. Despite the miscibility of PMMA with PEO, solvent casting proved to be a powerful technique to induce different morphologies including an amorphous state, micelles with a PMMA core and flower-like PEO chains on the exterior of the micelle, and a cross-linked gel. The nanostructure of thin films was studied through the combination of atomic force microscopy (AFM) and grazing incidence small-angle X-ray scattering (GISAXS).

2. Experimental section

2.1. Materials

Methyl methacrylate (MMA, Aldrich, 99%) was passed through an activated basic alumina column before use. CuBr (Acros, 98%) was purified according to a previously described procedure [53,54]. Toluene (Fisher, 99.8%), tetrahydrofuran (Fisher, 99.8%), and acetone (Fisher, 99.7%) were distilled and stored under nitrogen. Immediately before use, both monomers and solvents were purged with N_2 for at least 30 min. *N*,*N*,*N*′,*N*″,*N*″-Pentamethyldiethylenetriamine (PMDETA, Aldrich, 99%) was passed through a short column of alumina before use. Poly(ethylene glycol) ($M_n = 2000$ g/mol; $M_n =$ 20,000 g/mol; $M_n = 35{,}000$ g/mol) and poly(ethylene glycol) monomethyl ester ($M_n = 2000$ g/mol) were purchased from Aldrich. Unless specified, all other reagents were purchased from commercial sources and used without further purification.

2.2. Synthesis of poly(ethylene oxide) macroinitiators

Difunctional Br–PEG_{2000}–Br was synthesized by the dicyclohexyl carbodiimide (DCC) coupling method. To a dried 500 mL three-necked round bottom flask in an ice bath, equipped with a condenser and a dropping funnel, poly(ethylene glycol) (20.0 g, 10 mmol, $M_n = 2000$ g/mol), DCC (4.13 g, 20 mmol), and 4-dimethylaminopyridine (0.0244 g, 0.2 mmol) were dissolved in dichloromethane (270 mL). 2-Bromo-2-methylpropionic acid (3.34 g, 20 mmol), dissolved in dichloromethane (30 mL), was added dropwise over a period of 3 h. The

reaction mixture was allowed to react overnight at room temperature. After completion of the reaction, the solid dicyclohexyl urea byproduct was filtered off. Some of the dichloromethane was removed on the rotary evaporator. The product was washed with water three times, and the organic phase was isolated. The product was precipitated in hexanes twice, and dried overnight under vacuum; $M_n = 2400$ g/mol and PDI = 1.04. ^{1}H NMR (2.15 ppm, 12H, CH_3; 3.62 ppm, 188H, CH_2). In a similar manner, Br–$PEO_{20,000}$–Br and Br–$PEO_{35,800}$–Br were synthesized. Additionally, monofunctional Br–PEO_{2000}–Me was also prepared by starting with poly(ethylene glycol) monomethyl ester ($M_n = 2000$ g/mol).

2.3. ATRP of PMMA–PEO–PMMA

In a typical experiment, Br–PEG_{2000}–Br macroinitiator (1.0 g, 0.25 mmol), 2,2′-bipyridine (bpy) (0.078 g, 0.5 mmol), and $CuBr_2$ (0.0056 g, 0.025 mmol) were added to a dried Schlenk flask equipped with a stir bar. After sealing it with a rubber septum, the flask was degassed and backfilled with nitrogen three times and then left under nitrogen. Subsequently, methyl methacrylate (4.5 mL, 50 mmol) and acetone (20 mL) were added. The mixture was then frozen with liquid nitrogen and degassed by three freeze–pump–thaw cycles. After the third cycle, the flask was left frozen, and CuBr (0.071 g, 0.5 mmol) was added under N_2 flux. The flask was vacuumed and backfilled with N_2 before placing the vial in an oil bath and stirred at 50 °C for 17.5 h. The flask was removed from the oil bath, and the reaction was stopped by exposure to air and diluted with acetone. The solution was filtered through a column filled with neutral alumina to remove the catalyst, and the polymer (51% conversion) was recovered by precipitation in hexanes and dried in a vacuum at 40 °C to constant weight; $M_n = 10{,}700$ g/mol; $M_w/M_n = 1.21$.

2.4. Halogen exchange ATRP of PMMA–PEO–PMMA

The same procedure was followed as with normal ATRP, except that CuCl and $CuCl_2$ were used instead of CuBr and $CuBr_2$. For an experiment with CuCl (0.049 g, 0.5 mmol), Br–PEG_{2000}–Br macroinitiator (1.0 g, 0.25 mmol), bpy (0.078 g, 0.5 mmol), methyl methacrylate (4.5 mL, 50 mmol), acetone (20 mL), and $CuCl_2$ (0.0034 g, 0.025 mmol) at 50 °C for 26.5 h, the polymer (71% conversion) was recovered by precipitation in hexanes and dried in a vacuum at 40 °C to constant weight; $M_n = 14{,}300$ g/mol; $M_w/M_n = 1.17$.

2.5. Characterization

Monomer conversion was determined on a Shimadzu GC-17A gas chromatograph equipped with a flame ionization detector and a capillary column (CEC-Wax, 30 m × 0.53 mm × 1.0 μm, Chrom Expert Co.). Acetone or toluene, which was added initially to the reaction mixture, was used as an internal standard for these measurements.

Molecular weights and polydispersity indices (PDIs) were measured on a GPC system consisting of a Waters 515 pump, a Waters 717plus autoinjector, Polymer Standards Service 10^5 Å, 10^3 Å, and 10^2 Å columns, and a Waters 410 refractive index (RI) detector against poly(methyl methacrylate) standards. THF was used as eluent with a flow rate of 1 mL/min (30 °C).

^{1}H NMR spectra were recorded on a 500 MHz Bruker spectrometer, using $CDCl_3$ as a lock solvent and TMS as a standard.

Dynamic light scattering (DLS) measurements were performed using a Malvern Instruments High Performance Particle Sizer (HPPS) HPP5001.

Differential scanning calorimetric (DSC) experiments were performed with ~10 mg samples placed in sealed Al pans, using a Seiko SSC/5200 instrument operated under N_2 purge (30 mL/min) and cycled at 10 °C/min between −150 °C and 100 °C. In order to minimize the effects of previous thermal and rheological history, data from the third heating/cooling cycle were used in the analysis.

Wide-angle X-ray scattering (WAXS) was performed on a Philips PW 1840 X-ray diffractometer at room temperature using Cu Kα radiation in the angular (2θ) range of 10°–40°. Powders were placed in an aluminum sample holder.

Small-angle X-ray scattering (SAXS) was performed at room temperature with Cu Kα radiation using a compact Kratky Camera (Anton Paar) having a linear position-sensitive detector system with phase-height discrimination (Raytech) coupled to a multichannel analyzer (Nucleus). The entrance slit to the collimation block was 30 μm, and the slit length delimiters were set at 15 mm. The sample to detector distance was 26.4 cm. Sample powders were taped directly to the sample holder. The effects of solution processing were investigated by casting onto polyimide films. The scattering curves were corrected for sample absorption. The constant background, determined using a Porod plot, was subtracted. The correction for the effects of the geometry of a slit-collimated incident beam (desmearing) was performed using an indirect Fourier transformation procedure.

Grazing incidence small-angle X-ray scattering (GISAXS) was carried out with Cu Kα radiation using a wired detector. The sample was mounted on a motorized stage in order to control the incident angle and the sample azimuth. The exposure time under these conditions was 30 min. Data reported herein were obtained for the angle of incidence equal to 0.10°.

Tapping mode atomic force microscopic (TM-AFM) experiments were carried out using a Multimode Nanoscope III system (Digital Instruments, Santa Barbara, CA) equipped with a hot stage and fluid cell. The measurements were performed under ambient conditions using commercial Si cantilevers with a nominal spring constant and resonance frequency, respectively, equal to 40 N/m and 300 kHz. The height and phase images were acquired simultaneously at set-point ratio A/A_o between 0.7 and 0.9, where A and A_o refer to the "tapping" and "free" cantilever amplitudes, respectively. For AFM experiments in air, all of the polymer films were prepared by drop-casting from 1 mg/mL polymer solutions in chloroform, toluene, 1:1 water/THF, or water, followed by vacuum drying overnight at room temperature. AFM experiments under water were performed in a TM-AFM fluid cell.

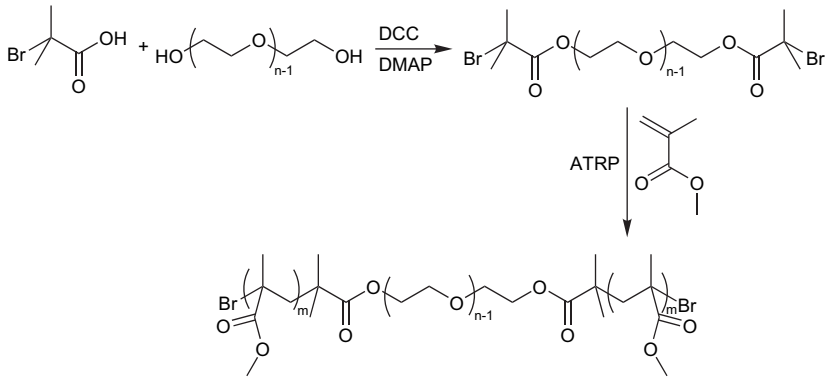

Scheme 1. Synthetic route to prepare PMMA-*b*-PEO-*b*-PMMA triblock copolymers by ATRP.

3. Results and discussion

3.1. Synthesis of PMMA–PEO–PMMA triblock copolymers by ATRP

Using different sized PEO macroinitiators various PMMA–PEO–PMMA triblock copolymers were synthesized using ATRP and halogen exchange ATRP (Scheme 1). For the preparation of these triblock copolymers, the ATRP reaction conditions were optimized (Table 1).

Different ratios of initiator to monomer as well as different ligands and copper halide systems were investigated. Employing bipyridine in acetone at 50 °C resulted in slightly better control, as compared to using PMDETA in toluene at 70 °C. Experiments using PMDETA showed low conversions and slow polymerization rates, due to the fact that PMDETA may be a too active ligand for methacrylates. Increasing the concentration of copper(I) with respect to the initiator helped to increase the rate of activation, pushing the equilibrium to the right. A decrease in the initiator to monomer ratio and the use of a less active ligand (bipyridine) resulted in higher

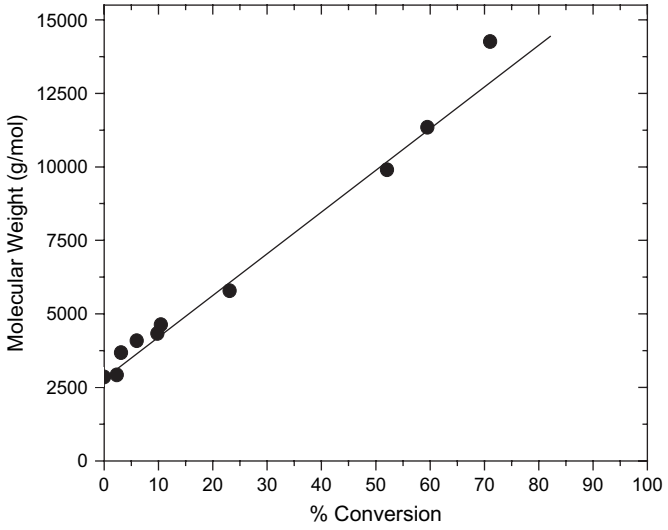

Fig. 1. Evolution of molecular weight vs. conversion for halogen exchange ATRP (Table 1, expt 3).

Table 1
ATRP reaction conditions for PMMA–PEO–PMMA triblock copolymers

Expt	Composition	M_n (g/mol) (GPC)	PDI	wt.% PEO	wt.% PMMA
1	PEO_{45}	2400	1.04	100	0
2[a]	$PMMA_{41}$–PEO_{45}–$PMMA_{41}$	10,700	1.21	19	81
3[b]	$PMMA_{59}$–PEO_{45}–$PMMA_{59}$	14,300	1.17	14	86
4	PEO_{470}	20,700	1.11	100	0
5[a]	$PMMA_{72}$–PEO_{470}–$PMMA_{72}$	35,200	1.15	59	41
6[b]	$PMMA_{52}$–PEO_{470}–$PMMA_{52}$	31,100	1.07	67	33
7	PEO_{805}	35,800	1.16	100	0
8[c]	$PMMA_{231}$–PEO_{805}–$PMMA_{231}$	82,000	1.21	43	57
9[c]	$PMMA_{116}$–PEO_{805}–$PMMA_{116}$	59,000	1.36	60	40
10[c]	$PMMA_{46}$–PEO_{805}–$PMMA_{46}$	44,000	1.27	80	20
11[d]	$PMMA_{76}$–PEO_{805}–$PMMA_{76}$	50,600	1.13	70	30
12[c]	$PMMA_{68}$–PEO_{805}–$PMMA_{68}$	40,000	1.38	88	8

All of the reactions were performed in acetone at 50 °C unless otherwise noted. The molar ratios are in parenthesis.

[a] PEO (0.5), MMA (100), CuBr (1), $CuBr_2$ (0.05), bpy (1).

[b] PEO (0.5), MMA (100), CuCl (1), $CuCl_2$ (0.05), bpy (1).

[c] PEO (0.5), MMA (400), CuBr (1), $CuBr_2$ (0.05), PMDETA (1); solvent: toluene; 70 °C.

[d] PEO (0.5), MMA (400), CuBr (1), $CuBr_2$ (0.05), bpy (1).

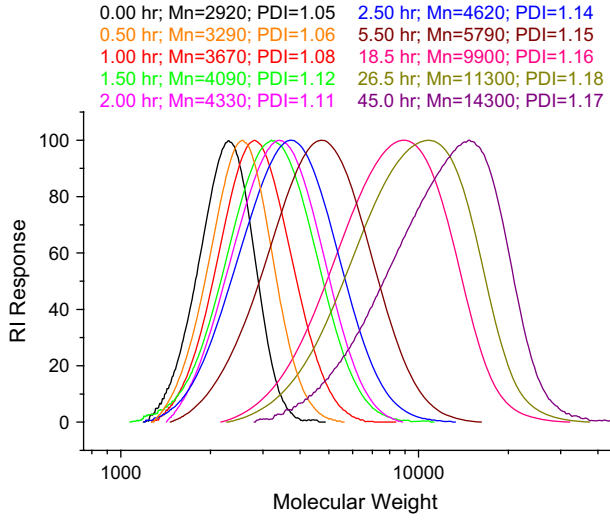

Fig. 2. Evolution of molecular weight for halogen exchange ATRP (Table 1, expt 3), as measured by GPC.

conversion and better control, especially for the smaller PEO macroinitiators.

Halogen exchange [55–57] is useful for the preparation of block copolymers when chain extension is occurring from a macroinitiator of lower activity to a more active monomer. The procedure works because the rate of activation of a 2-bromoisobutyrate PEO chain end is faster than the activation of a chloro-terminated polymethacrylate chain end. The R–Br bond is readily activated using a CuCl catalyst, therefore initiation is a fast process [23,40]. After initiation, however, most of the dormant chains have a terminal chlorine atom because the C–Cl bond is stronger than the C–Br bond. These C–Cl bonds are activated more slowly, and thus the rate of propagation is decreased with respect to the rate of initiation, which effectively leads to increased initiation efficiency and the preparation of a second block with lower polydispersity.

The normal ATRP and halogen exchange ATRP systems were compared for the synthesis of PMMA–PEO–PMMA copolymers. As expected with bpy as the ligand, the halogen exchange reactions were slower. Since the rate of propagation is slower ($k_{p,app}$ (for CuCl system) < $k_{p,app}$ (for CuBr system)), the halogen exchange reactions were better controlled. Evolution of molecular weight vs. conversion for the halogen exchange system is presented in Fig. 1. In comparing experiments 2 and 3 in Table 1, the PDI is lower for the reaction using halogen exchange. Both of these reactions were run using the same macroinitiator and identical conditions, the only difference being the metal halide. The reactions went to over 80% completion, and yielded polymers with low polydispersity. The increase of molecular weight with respect to % conversion was better controlled for the halogen exchange reaction. A comparison of experiments 5 and 6 demonstrates

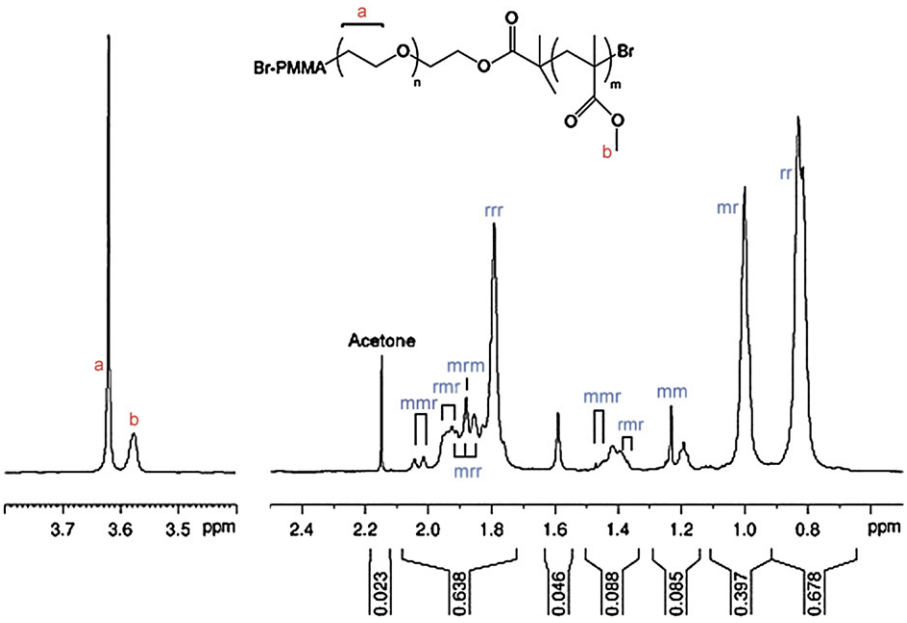

Fig. 3. ^{1}H NMR spectrum of syndiotactic $PMMA_{100}$–PEO_{858}–$PMMA_{100}$ (Table 1, expt 9).

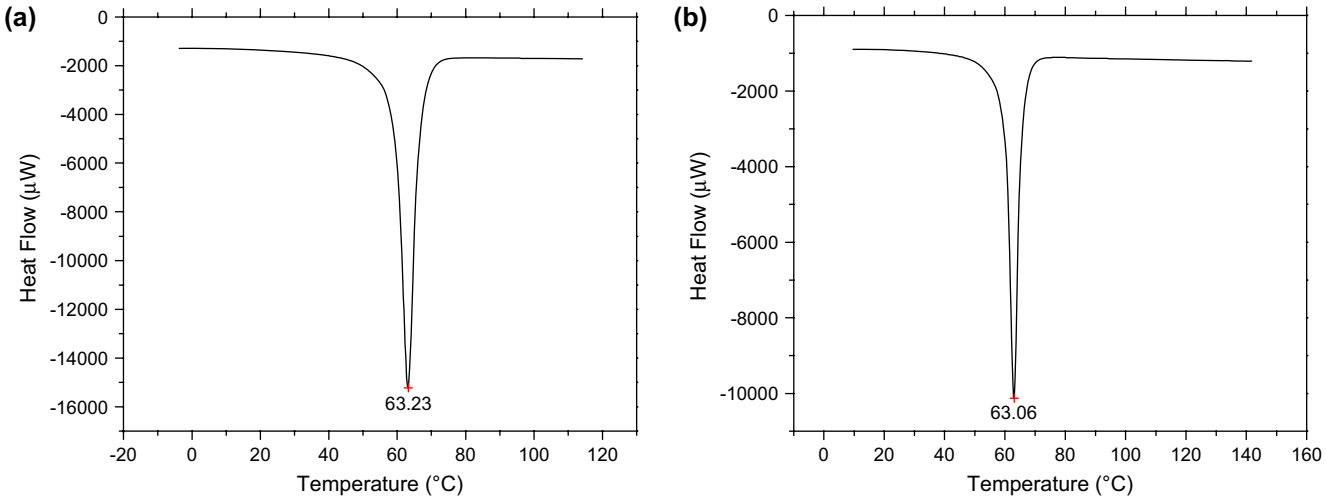

Fig. 4. DSC traces for (a) PEO macroinitiator and (b) $PMMA_{221}$–PEO_{858}–$PMMA_{221}$.

the same trend. GPC traces (Fig. 2) for the halogen exchange reaction reveal a smooth evolution of molecular weight with time where the polydispersity remains low.

^{1}H NMR analysis confirmed that MMA incorporates in a predominantly syndiotactic fashion, as expected for a radical process [58] (Fig. 3). The M_n calculated by GPC ($M_n = 59{,}000$ g/mol) and NMR ($M_n = 57{,}800$ g/mol) is in good agreement.

Further ^{1}H NMR characterization was performed on samples with smaller PEO segments to better characterize the materials. For $PMMA_{63}$–PEO_{45}–$PMMA_{63}$ (Table 1, expt 3), a comparison of the PEO CH_2 peak a with the PMMA methoxy peak b shows that there are approximately 59 units of MMA on each side of the PEO center block. Therefore, the NMR-calculated M_n of the PMMA portion is 12,760 g/mol, and the total M_n is 14,760 g/mol, which agrees well with the GPC value of 14,300 g/mol.

3.2. Differential scanning calorimetry (DSC)

Based on DSC analysis, the melting temperature of the PEO block in the high molecular weight copolymer $PMMA_{221}$–PEO_{858}–$PMMA_{221}$ ($T_m = 63.06$ °C) was very close to the melting temperature of comparable homopolymer PEO_{858} ($T_m = 63.23$ °C) (Fig. 4). The T_g of PMMA (100–120 °C) was not observed for this sample containing large PEO and short PMMA blocks.

For a sample with shorter PMMA blocks, $PMMA_{76}$–PEO_{805}–$PMMA_{76}$, $M_n = 50{,}600$ g/mol, 30% PMMA, 70% PEO, the T_g for PEO was observed around −42 °C, which is higher than the literature value of pure PEO (−64 °C) due to the influence of the PMMA segments. The T_m of the copolymer was also observed at 58.4 °C. The T_g for PMMA was not observed due to the high proportion of PEO in the copolymer (Fig. 5).

DSC analysis was also performed on a lower molecular weight sample with higher PMMA content ($PMMA_{59}$–PEO_{45}–$PMMA_{59}$, $M_n = 14{,}260$ g/mol, 83% PMMA, 17% PEO). The

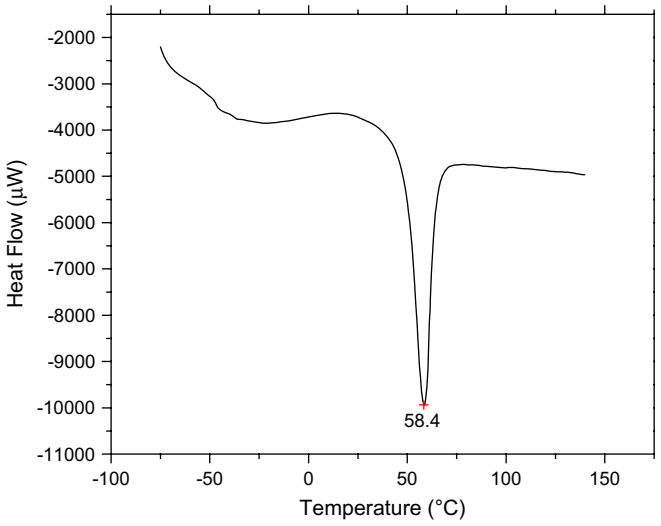

Fig. 5. DSC traces for $PMMA_{76}$–PEO_{805}–$PMMA_{76}$.

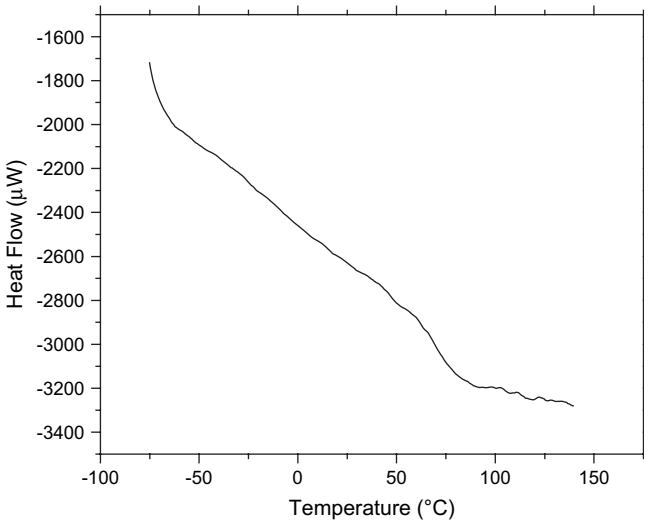

Fig. 6. DSC curve for $PMMA_{59}$–PEO_{45}–$PMMA_{59}$.

DSC trace for this sample, shown in Fig. 6, exhibited an ill-defined feature at −50 °C due to the phase transition of PEO and a strong feature at 75 °C, which could be related to the glass transition of the PMMA block. It is also of note that this sample did not exhibit PEO melting, as has been previously observed [33].

3.3. Triblock copolymer structure and crystallinity of PEO

PEO is a monoclinic crystal with a, b, c and β_c of about 8.0 Å, 13.0 Å, 19.5 Å and 125°, respectively. All of the triblock copolymers exhibited two main WAXS peaks at $2\theta = 19.34°$ and 23.46° that are typical of PEO and correspond, respectively, to spacings $d_{120} = 4.56$ Å and $d_{112,320} = 3.76$ Å. By fitting the WAXS profiles with a combination of possible crystalline peaks as well as the amorphous phase with Gaussian curves, we were able to separate the peaks contributed by the crystalline phase of PEO from broad halos originating from the amorphous phase of PEO and of PMMA (Fig. 7). The deconvolution was carried out in Mathematica 5.2 (Wolfram Research) using custom written procedures. The shape and the position of the curves fitting the amorphous halos of PMMA used in the deconvolution procedure were based on the measurement of the PMMA homopolymer. The shape of the PEO amorphous halo was taken from the literature [59]. The crystallinities of the PEO blocks were then calculated as the ratio $A_c/(A_c + A_a)$, where A_c denotes the area under the crystalline peaks of PEO and A_a is the area under its amorphous halo. The crystallinities determined in this way agreed to within 2% with the values based on the DSC analysis. The PEO crystallinity was generally lower in copolymers and increased with the PEO content.

The lateral sizes of the PEO crystallites were calculated from the shape of (120) peak using the Scherrer equation [60]:

$$B = 0.9\lambda/(t\cos\theta)$$

where B is the full width at half height of the scattering peak, λ is the wavelength of the X-ray beam, t is the grain size, and θ is the scattering angle. The PEO crystallite size in the block

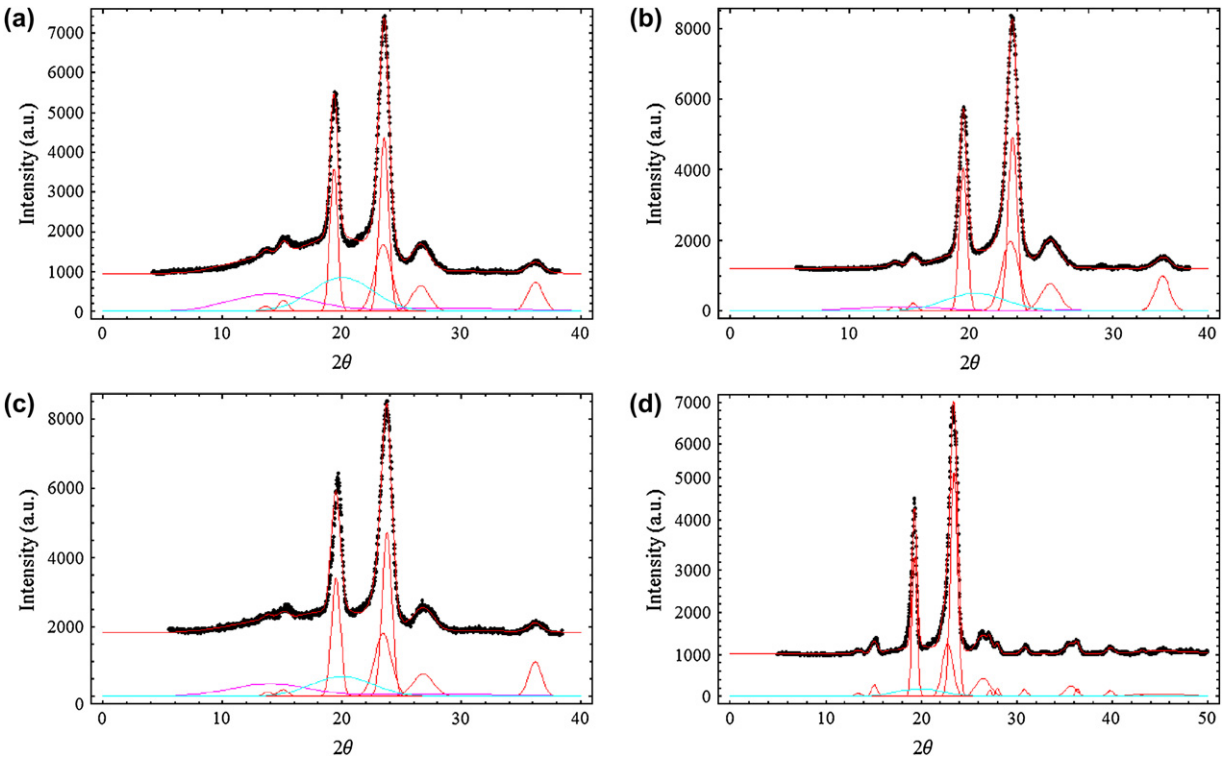

Fig. 7. Experimentally observed (black dots) and fitted (colored lines) WAXS patterns: (a) MPEO = 72%, (b) MPEO = 80%, (c) MPEO = 88%, and (d) homopolymer PEO. (For interpretation of the references to color in this figure legend, the reader is referred to the web version of this article.)

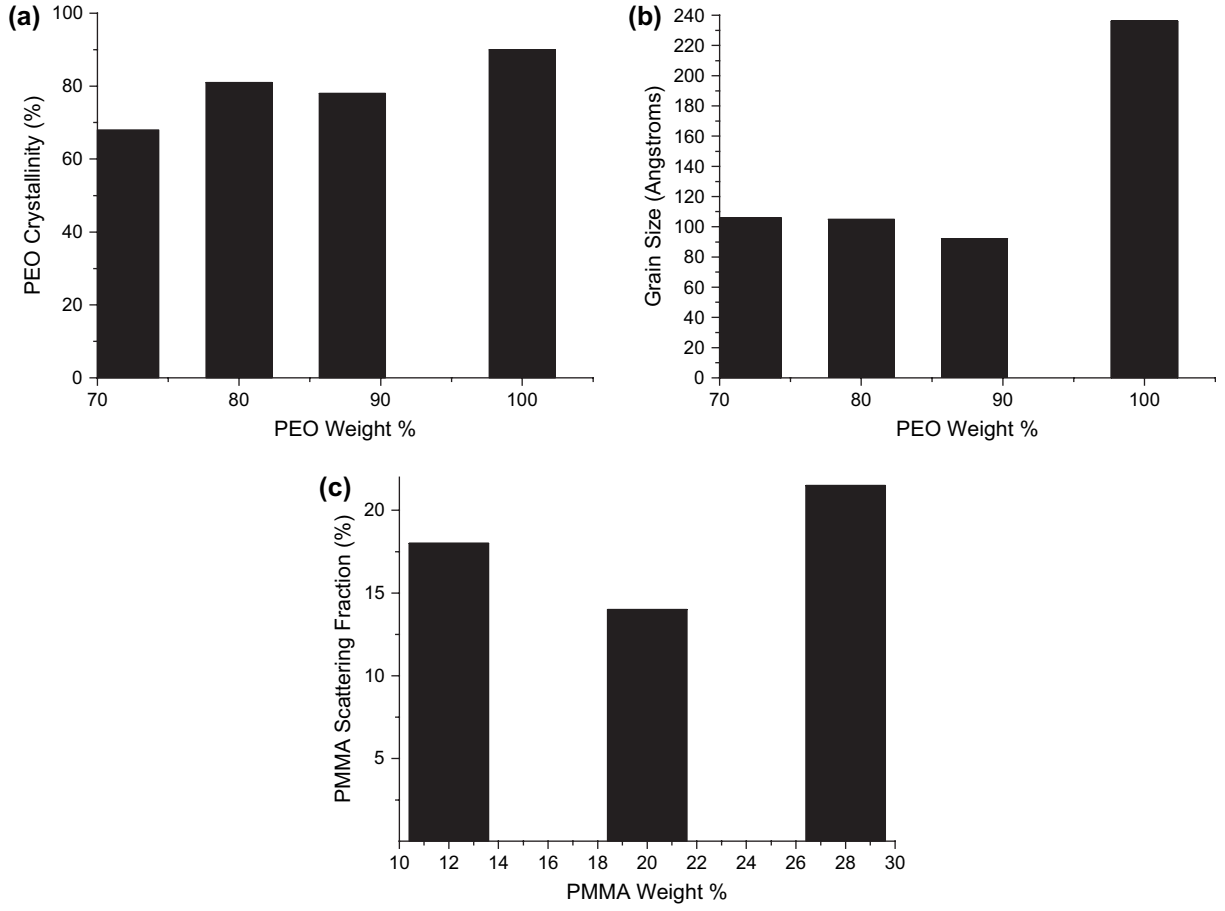

Fig. 8. (a) PEO crystallinity vs. PEO weight content, (b) PEO crystal grain sizes vs. PEO weight content, and (c) PMMA scattering fraction (ratio of the area under the PMMA halo to the total area under the diffraction) vs. PMMA weight content.

copolymers was found to be about two times smaller than the one observed for PEO in the homopolymer (Fig. 8b), suggesting the lateral segmentation of the PEO crystallites due to the rejection of flanking PMMA blocks from the lamellae. Such proposed fragmentation of PEO lamellae is consistent with the results of SAXS experiments on bulk samples, which did not show any evidence of periodicities typically observed for lamellar morphologies in partially crystalline polymers. For all copolymer compositions, the lateral sizes of PEO crystallites remained close to each other within 10%, pointing to the relatively low impact of the length of the flanking PMMA blocks on their rejection pattern from the PEO crystallites (Fig. 8).

By deconvoluting the WAXS profiles of the block copolymers, we were also able to identify the intensity of scattering contributed by the amorphous PMMA. The PMMA scattering fraction increased with the PMMA content as shown in Fig. 8c.

3.4. Surface and solvent induced morphologies of PMMA-b-PEO-b-PMMA triblock copolymers

The surface morphology of the triblock copolymers was investigated with the help of TM-AFM. TM-AFM is a powerful tool for providing not only topographical information about the sample surface (height image), but also mapping of regions with different levels of energy dissipation during tip–sample intermittent contacts (phase imaging). TM-AFM has also been shown to be particularly useful in visualizing the surface morphology of block copolymers and discrete nanoobjects at a nanometer scale [61,62]. Upon drop-casting from chloroform, the sample containing 70 wt.% PEO (Table 1, expt 11) formed stacked lamellar structures with the average height of lamellar steps equal to 4 nm formed by the crystallization of the PEO block, as shown in Fig. 9. These structures are consistent with a lamellar morphology, as expected for the partially crystalline PEO phase. The sample was then heated to 70 °C under N_2 with the help of a hot stage, kept at this temperature for 10 min, and then cooled down to 40 °C. Following this treatment, the lamellar stacks were no longer apparent on the surface. Instead, the surface of the film was covered with a ~10 nm thick dendritic layer, presumably corresponding to the recrystallized PEO lamellae parallel to the surface (Fig. 10a and b). There were no indications of bulk phase separation between PMMA and PEO, consistent with their partial miscibility [27].

The structures of the triblock copolymers were further elucidated by GISAXS, as shown in Fig. 11. The GISAXS pattern of homopolymer PEO exhibited an isotropic scattering ring corresponding to a spacing of 21.6 nm (Fig. 11a). One of the possible reasons why the vertical spacing measured by AFM was only about one half of the lamellar spacing observed by GISAXS is that the steps at the edges of the lamellae did not extend all the way through to the top of underlying lamellae, e.g. due to the presence of the amorphous layer. It is also possible that the lamellae near the surface were simply thinner than those in the bulk. The GISAXS pattern of the triblock copolymer $PMMA_{76}$–PEO_{805}–$PMMA_{76}$ (Fig. 11b) also showed the scattering maximum, which corresponded to the spacing of

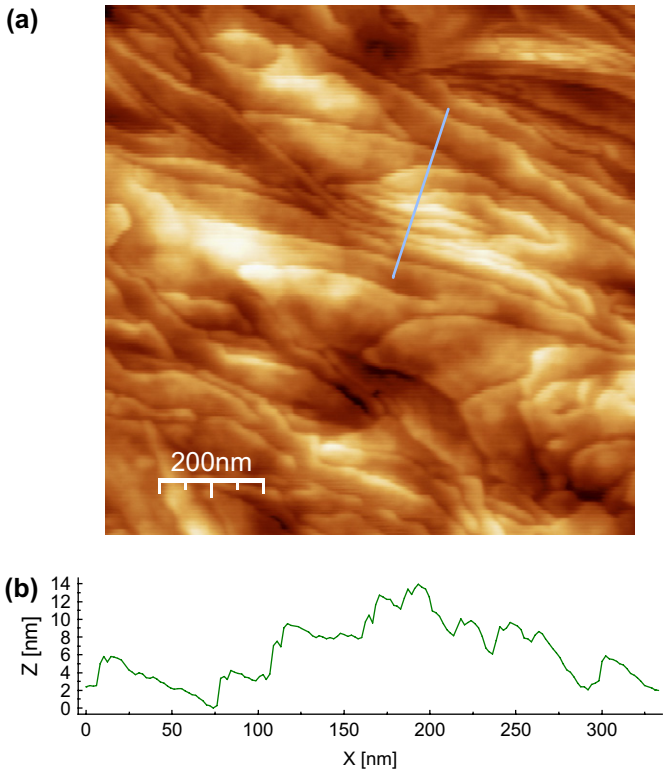

Fig. 9. TM-AFM of $PMMA_{76}$–PEO_{805}–$PMMA_{76}$ drop-cast from chloroform at room temperature: (a) height image and (b) cross-section profile taken along the line indicated in (a).

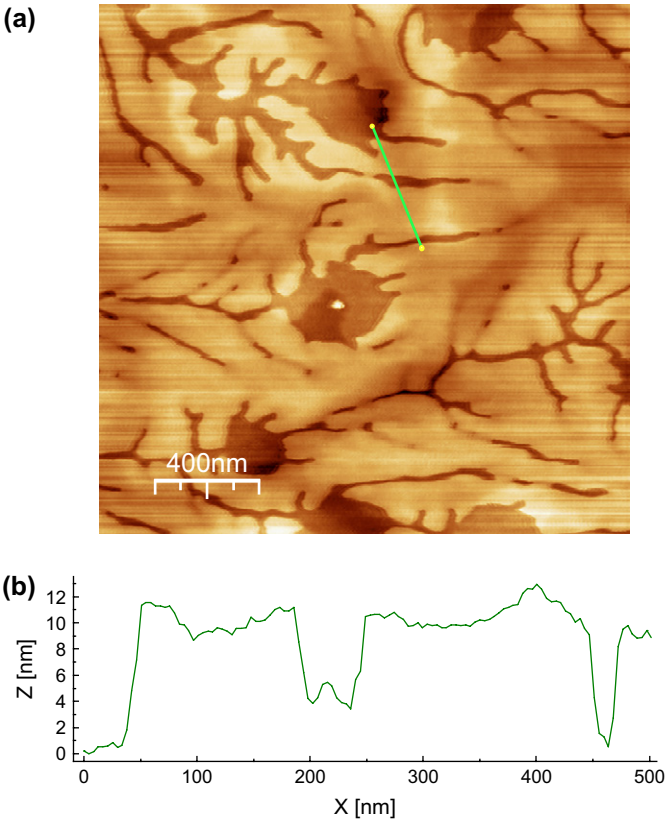

Fig. 10. TM-AFM of $PMMA_{76}$–PEO_{805}–$PMMA_{76}$ drop-cast from chloroform at room temperature and annealed at 70 °C for 10 min: (a) height image and (b) cross-section profile at the line indicated in (a).

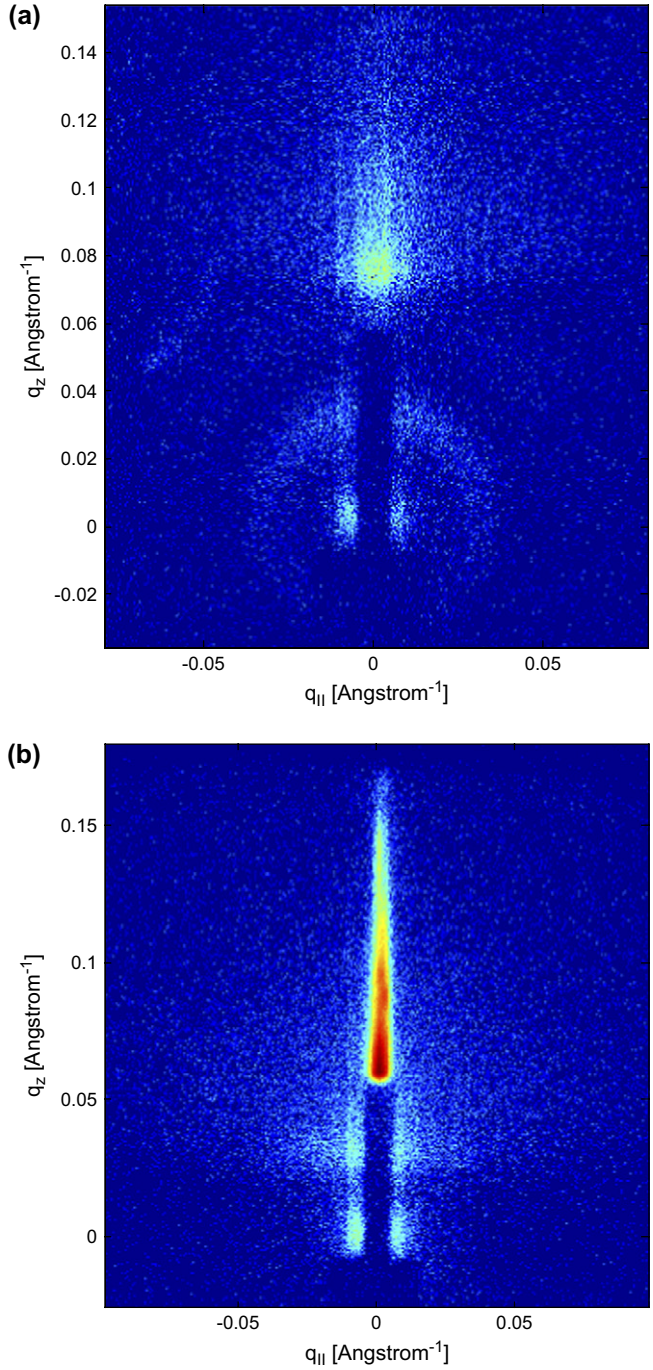

Fig. 11. GISAXS patterns for (a) PEO homopolymer and (b) $PMMA_{76}$–PEO_{805}–$PMMA_{76}$.

21.4 nm. However, in this case, the scattering pattern was highly anisotropic and indicated that the lamellae were oriented parallel to the surface. It is worth pointing out that the periodicity observed by GISAXS in thin films of the block copolymers was not observed in transmission SAXS of the bulk powder samples. One of the possible explanations of this discrepancy is the surface induced ordering of fragmented PEO crystallites in thin films.

Block copolymers placed in a solvent strongly selective to one of the blocks may assemble into a variety of structures [63,64]. Herein, the micellization of the PMMA–PEO–PMMA triblock copolymer was induced by gradually adding water to a THF polymer solution. THF was chosen as a good solvent for both blocks, while water is a preferential solvent for PEO. The sample $PMMA_{76}$–PEO_{805}–$PMMA_{76}$ was first dissolved in THF to concentration of 1 mg/mL, followed by dilution with water until a 1:1 (v:v) THF/water ratio was achieved. The suspension was then drop-cast onto a silicon substrate. TM-AFM imaging revealed the presence of uniform globular aggregates with an average diameter of ~35 nm (Fig. 12). Dynamic light scattering (DLS) measurement of this block copolymer in THF/water showed the presence of aggregates with an average hydrodynamic radius of ~320 nm. This value corresponds very closely to the size of fully extended PEO chains with DP 805 ($L = 363$ nm), suggesting that the measured size is twice that of half looped PEO chains. DLS of the same block copolymer in chloroform showed only the presence of solvated individual copolymer chains (average hydrodynamic radius of 17 nm).

Since water is a non-solvent for PMMA, the observed micelles were expected to consist of PMMA cores and flower-like PEO corona. Variable temperature TM-AFM measurement provided support for this type of core–shell structure. It has been demonstrated that thermal transitions (melting/crystallization, vitrification/devitrification) can be followed by monitoring the phase shift at different temperatures [65]. Phase images acquired at two different temperatures 26 °C and 60 °C are shown in Fig. 13. At room temperature, both PMMA and PEO are mechanically less lossy than the substrate, probably because a moisture layer was formed on the silicon dioxide surface. When the temperature was increased to 60 °C, the phase images revealed the presence of distinct core–shell structure. The dark shells of

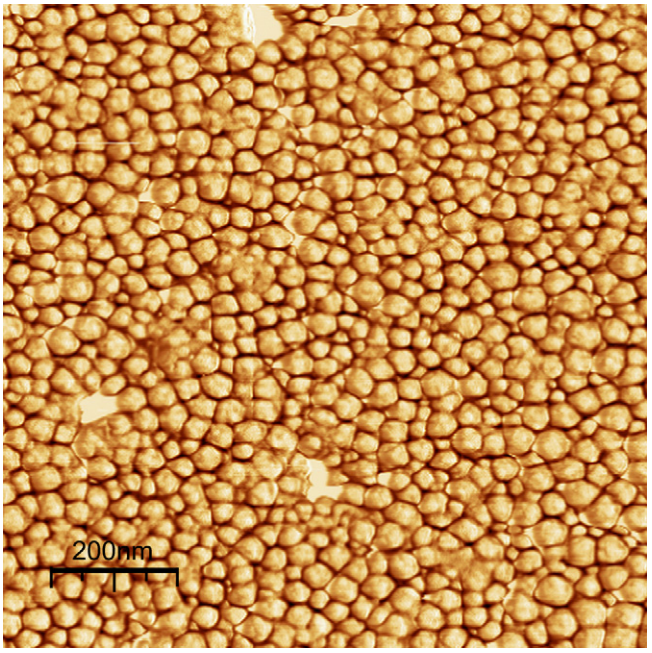

Fig. 12. TM-AFM phase image of $PMMA_{76}$–PEO_{805}–$PMMA_{76}$ drop-cast from THF/water mixed solvent (1:1, v:v).

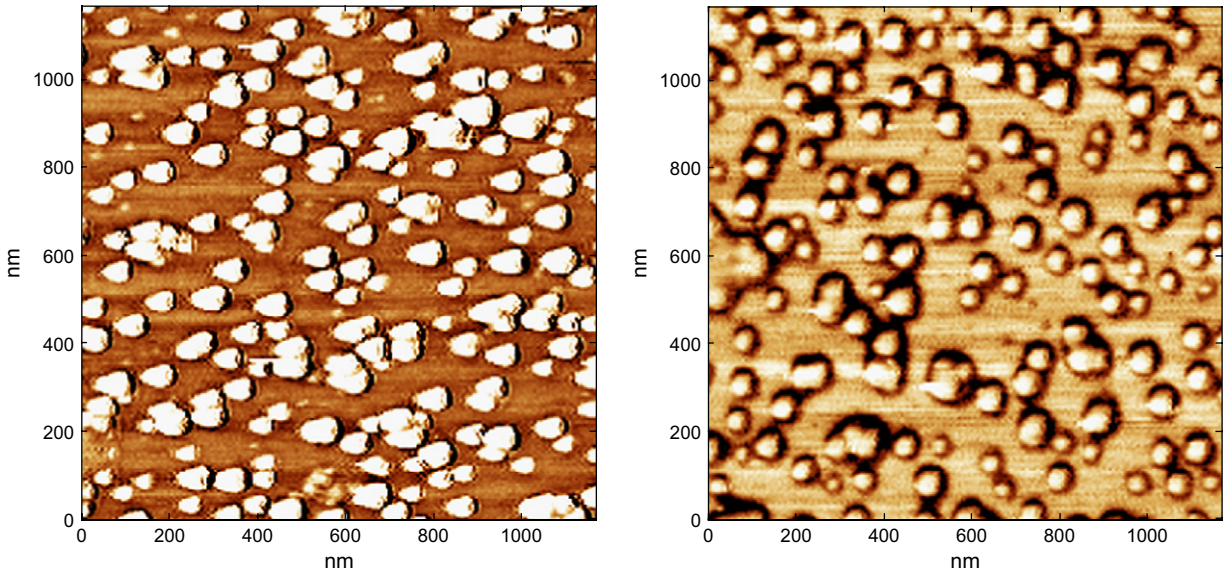

Fig. 13. TM-AFM phase images of $PMMA_{76}$–PEO_{805}–$PMMA_{76}$ acquired at 26 °C and 60 °C, by drop-casting from 1:1 THF/water.

the more mechanically lossy molten PEO were surrounded by the lighter cores of the glassy PMMA.

It is particularly interesting to investigate how the micelles behave in an aqueous media, for their compatibility in a biological system may be important for potential use as a drug delivery system. To aid in an understanding of the micelles in such an environment, the block copolymer micelles were studied under water using TM-AFM (Fig. 14).

When the samples were imaged under water, the number of micelles per unit area was considerably lower than in the dry state, most likely due to the release of the weakly attached micelles from the substrate and their transfer into the liquid. The

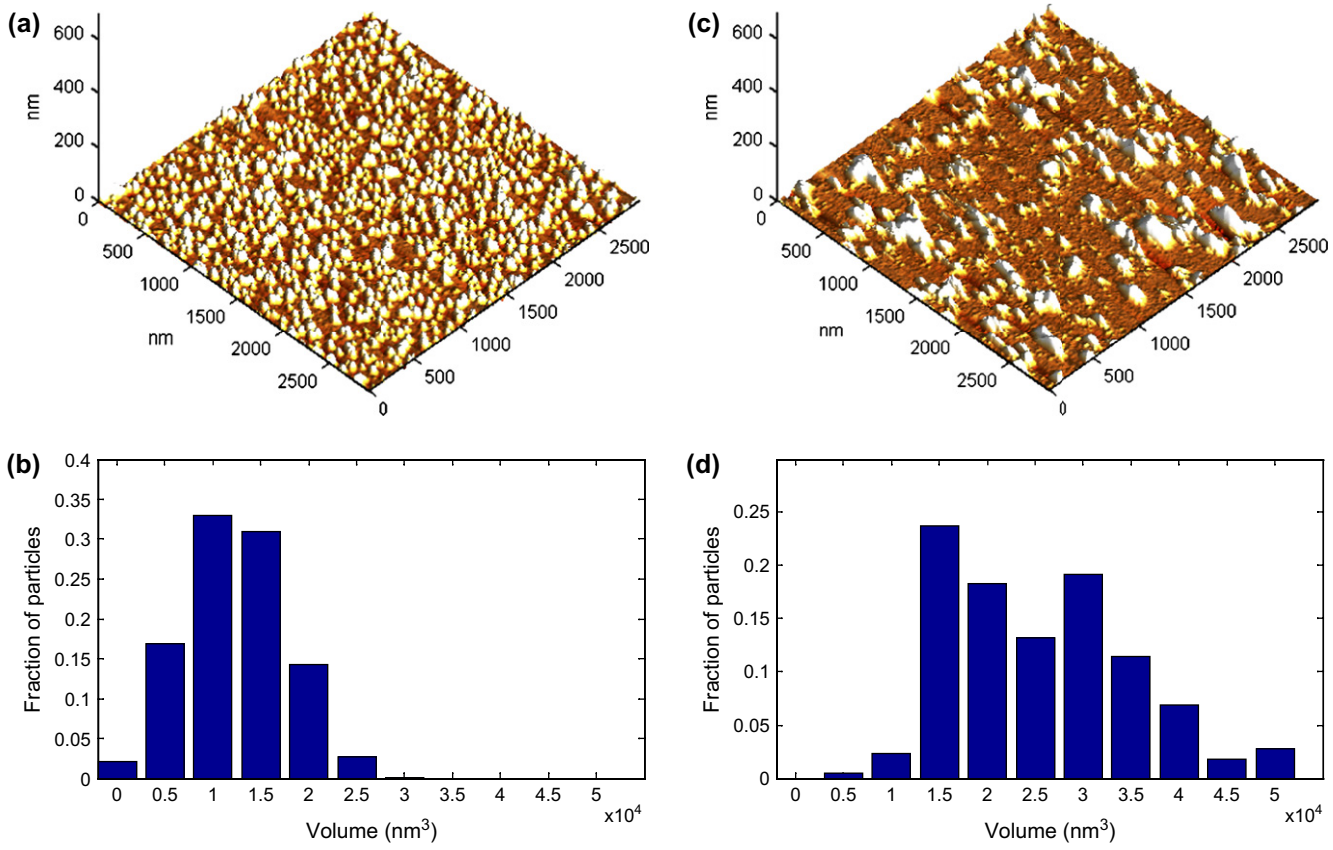

Fig. 14. TM-AFM imaging of $PMMA_{76}$–PEO_{805}–$PMMA_{76}$, cast from 1:1 THF/water. Left: (a) height image and (b) particle volume distribution for the sample imaged in air. Right: (c) height image and (d) particle volume distribution for sample imaged under water.

average size of the micelles increased from ~35 nm to ~45 nm due to the solvation of the PEO shell, and their average volume increased from 1×10^4 nm^3 to 2.5×10^4 nm^3. Assuming that a dry particle has a diameter of 35 nm and density 1 g/cm^3, this would correspond to a molecular weight of 14.2×10^6 g/mol. By dividing this value by the MW of a single chain (50,600 g/mol), an aggregation number of 280 chains/particle was obtained. The reason for lower numbers of micelles in the AFM image could be dissolution of some of the spheres, due to the weak physical attachment to the surface. This effect could be enhanced by the interaction with the AFM tip.

Interestingly, one simple solvent casting technique could produce different morphologies, depending if a single solvent or a mixed solvent was used. It is also noteworthy that fast addition of water to the micellar samples induced formation of a gel. Some hydration studies were performed on the same sample that formed both stacked lamellar structures and flower-like micelles with PMMA cores. When $PMMA_{76}$–PEO_{805}–$PMMA_{76}$ was cast from 1:1 THF/water, ~36 nm dry spheres were visualized by AFM. For the same sample, ~300 nm spheres were seen by DLS when swollen in water. Fast addition of water allowed for the formation of a 5 wt.% gel. After hydration overnight in an excess of water, the gel was removed, lightly patted dry with paper and weighed to estimate the amount of water absorbed by the gel. When the gel was first dried and then hydrated in an excess of water, 40.8 g of water was absorbed by 1 g of gel. If instead, the 5 wt.% wet gel was hydrated overnight without drying, then 250 g of water could be absorbed by 1 g of gel. As previously suggested [39], PMMA–PEO–PMMA copolymers are highly water swellable and might be applicable for use as highly permeable biocompatible encapsulating materials for mammalian cells.

4. Conclusion

In this article, we described the controlled synthesis of PMMA–PEO–PMMA triblock copolymers by ATRP. PEO-based macroinitiators with molecular weight from 2000 to 35,800 g/mol were used to initiate the polymerization of MMA to obtain copolymers with molecular weight up to 82,000 g/mol and polydispersity index (PDI) less than 1.2. The lateral sizes of PEO crystallites of block copolymers determined from WAXS were found to be half of the size of PEO crystallites in the homopolymer, suggesting lateral segmentation of the PEO lamellae due to the rejection of flanking PMMA blocks from the lamellae. In thin films, fragmentation of lamellae appeared to be at least partially overcome by substrate induced ordering, as evidenced in AFM images and GISAXS pattern. It has also been found that solvent casting can alter the morphology of the block copolymers, permitting the formation of either lamellae or spheres for the same sample. Because these materials are highly water swellable, they might find application as permeable biocompatible encapsulating materials for mammalian cells or for use in contact lenses. The micellar form might be applicable to drug delivery. *In vitro* cytotoxicity studies of this material are underway, and the results will be described in a future publication.

Acknowledgements

The authors would like to acknowledge the financial support from the CRP Consortium, the National Tissue Engineering Center Grant DAMA 17-02-0717, the National Institutes of Health Grant RO1 DE15392, the National Science Foundation Grant NSF-05-49353, CBET 05 21079, and the United States – Israel Binational Science Foundation.

References

[1] Wang JS, Matyjaszewski K. J Am Chem Soc 1995;117:5614–5.
[2] Tsarevsky NV, Matyjaszewski K. Chem Rev 2007;107:2270–99.
[3] Matyjaszewski K, Xia JH. Chem Rev 2001;101:2921–90.
[4] Kamigaito M, Ando T, Sawamoto M. Chem Rev 2001;101:3689–745.
[5] Matyjaszewski K, Davis TP. Handbook of radical polymerization. Hoboken: Wiley-Interscience; 2002.
[6] Braunecker WA, Matyjaszewski K. Prog Polym Sci 2007;32:93–146.
[7] Matyjaszewski K, Gnanou Y, Leibler L, editors. Macromolecular engineering: from precise macromolecular synthesis to macroscopic materials properties and applications. Weinheim: Wiley-VCH; 2007.
[8] Wang J-S, Matyjaszewski K. Macromolecules 1995;28:7901–10.
[9] Pyun J, Tang C, Kowalewski T, Frechet JMJ, Hawker CJ. Macromolecules 2005;38:2674–85.
[10] Qin S, Saget J, Pyun J, Jia S, Kowalewski T, Matyjaszewski K. Macromolecules 2003;36:8969–77.
[11] Pietrasik J, Bombalski L, Cusick B, Huang J, Pyun J, Kowalewski T, et al. ACS Symp Ser 2005;912:28–42.
[12] Beers KL, Gaynor SG, Matyjaszewski K, Sheiko SS, Moeller M. Macromolecules 1998;31:9413–5.
[13] Davis KA, Matyjaszewski K. Adv Polym Sci 2002;159:1–169.
[14] Matyjaszewski K. Polym Int 2003;52:1559–65.
[15] Matyjaszewski K. Prog Polym Sci 2005;30:858–75.
[16] Arehart SV, Matyjaszewski K. Macromolecules 1999;32:2221–31.
[17] Lutz J-F, Neugebauer D, Matyjaszewski K. J Am Chem Soc 2003;125:6986–93.
[18] Matyjaszewski K, Ziegler MJ, Arehart SV, Greszta D, Pakula T. J Phys Org Chem 2000;13:775–86.
[19] Coessens V, Pintauer T, Matyjaszewski K. Prog Polym Sci 2001;26:337–77.
[20] Shipp DA, Wang JL, Matyjaszewski K. Macromolecules 1998;31:8005–8.
[21] Wu W, Huang J, Jia S, Kowalewski T, Matyjaszewski K, Pakula T, et al. Langmuir 2005;21:9721–7.
[22] Davis KA, Matyjaszewski K. Macromolecules 2001;34:2101–7.
[23] Hadjichristidis N, Iatrou H, Pitsikalis M, Mays J. Prog Polym Sci 2006;31:1068–132.
[24] Pearce R, Vancso GJ. J Polym Sci Part B Polym Phys 1998;36:2643–51.
[25] Jin X, Zhang SH, Runt J. Macromolecules 2004;37:8110–5.
[26] Liau WB, Chang CF. J Appl Polym Sci 2000;76:1627–36.
[27] Colby RH. Polymer 1989;30:1275–8.
[28] Dionisio M, Fernandes AC, Mano JF, Correia NT, Sousa RC. Macromolecules 2000;33:1002–11.
[29] Richardson PH, Richards RW, Blundell DJ, Macdonald WA, Mills P. Polymer 1995;36:3059–69.
[30] Ahn SH, An JH, Lee DS, Kim SC. J Polym Sci Part B Polym Phys 1993;31:1627–39.
[31] Strobl G. Prog Polym Sci 2006;31:398–442.
[32] Kretzschmar H, Donth EJ, Tanneberger H, Garg D, Horing S. Thermochim Acta 1985;93:151–4.
[33] Shach-Caplan M, Silverstein MS, Bianco-Peled H, Tsarevsky NV, Cooper BM, Matyjaszewski K. Polymer 2006;47:6673–83.

[34] Sawhney AS, Pathak CP, Hubbell JA. Macromolecules 1993;26:581–7.
[35] West JL, Hubbell JA. React Polym 1995;25:139–47.
[36] Hillwest JL, Chowdhury SM, Slepian MJ, Hubbell JA. Proc Natl Acad Sci USA 1994;91:5967–71.
[37] Elisseeff J, Anseth K, Sims D, McIntosh W, Randolph M, Langer R. Proc Natl Acad Sci USA 1999;96:3104–7.
[38] Kim SH, Misner MJ, Xu T, Kimura M, Russell TP. Adv Mater 2004;16:226.
[39] Eisa T, Sefton MV. Biomaterials 1993;14:755–61.
[40] Nanda AK, Matyjaszewski K. Macromolecules 2003;36:8222–4.
[41] Ando T, Kamigaito M, Sawamoto M. Tetrahedron 1997;53:15445–57.
[42] Bernaerts KV, Du Prez FE. Prog Polym Sci 2006;31:671–722.
[43] Krishnan R, Srinivasan KSV. J Appl Polym Sci 2005;97:989–1000.
[44] Sun X, Zhang H, Zhang L, Wang X, Zhou Q-F. Polym J 2005;37:102–8.
[45] Sun X, Zhang H, Huang X, Wang X, Zhou Q-F. Polymer 2005;46:5251–7.
[46] Krishnan R, Srinivasan KSV. J Macromol Sci 2005;A42:495–508.
[47] Reining B, Keul H, Hocker H. Polymer 2002;43:3139–45.
[48] Angot S, Taton D, Gnanou Y. Macromolecules 2000;33:5418–26.
[49] Ramakrishnan A, Dhamodharan R. Macromolecules 2003;36:1039–46.
[50] Jiang J, Tong X, Zhao Y. J Am Chem Soc 2005;127:8290–1.
[51] Cheng SY, Xu ZS, Yuan JJ. Acta Chim Sin 2000;58:368–70.
[52] Xu ZS, Feng LX, Ji J, Cheng SY, Chen YC, Yi CF. Eur Polym J 1998;34:1499–504.
[53] Matyjaszewski K, Patten TE, Xia JH. J Am Chem Soc 1997;119:674–80.
[54] Xia J, Matyjaszewski K. Macromolecules 1999;32:2434–7.
[55] Matyjaszewski K, Shipp DA, Wang JL, Grimaud T, Patten TE. Macromolecules 1998;31:6836–40.
[56] Yagci Y, Tasdelen MA. Prog Polym Sci 2006;31:1133–70.
[57] Matyjaszewski K, Shipp DA, McMurtry GP, Gaynor SG, Pakula T. J Polym Sci Part A Polym Chem 2000;38:2023–31.
[58] Schilling FC, Bovey FA, Bruch MD, Kozlowski SA. Macromolecules 1985;18:1418–22.
[59] Chen EQ, Weng X, Zhang AQ, Mann I, Harris FW, Cheng SZD, et al. Macromol Rapid Commun 2001;22:611–5.
[60] Warren BE. X-ray diffraction. Dover Publications; 1 June 1990.
[61] Pearce R, Vancso GJ. Macromolecules 1997;30:5843–8.
[62] Guo QP, Thomann R, Gronski W, Staneva R, Ivanova R, Stuhn B. Macromolecules 2003;36:3635–45.
[63] Konak C, Helmstedt M. Macromolecules 2003;36:4603–8.
[64] Lai CJ, Russel WB, Register RA. Macromolecules 2002;35:841–9.
[65] Wu W, Matyjaszewski K, Kowalewski T. Langmuir 2005;21:1143–8.